

Safe Interval RRT* for Scalable Multi-Robot Path Planning in Continuous Space

Joonyeol Sim¹, Joonkyung Kim¹, Changjoo Nam¹

¹Sogang University, Republic of Korea
jysim@u.sogang.ac.kr, jkkim@u.sogang.ac.kr, cnam@sogang.ac.kr

Abstract

In this paper, we consider the problem of Multi-Robot Path Planning (MRPP) in continuous space. The difficulty of the problem arises from the extremely large search space caused by the combinatorial nature of the problem and the continuous state space. We propose a two-level approach where the low level is a sampling-based planner *Safe Interval RRT** (SI-RRT*) that finds a collision-free trajectory for individual robots. The high level can use any method that can resolve inter-robot conflicts where we employ two representative methods that are Prioritized Planning (SI-CPP) and Conflict Based Search (SI-CCBS). Experimental results show that SI-RRT* can quickly find a high-quality solution with a few samples. SI-CPP exhibits improved scalability while SI-CCBS produces higher-quality solutions compared to the state-of-the-art planners for continuous space.

Introduction

Multi-Robot Path Planning (MRPP) is the problem of finding collision-free paths for multiple robots while optimizing a given objective, such as the total path length (i.e., sum of costs) or the time taken to complete all tasks (i.e., makespan) (Stern et al. 2019), even in congested environments as shown in Fig. 1. While the problem has significant real-world applications like warehouse automation (Varambally, Li, and Koenig 2022) and search and rescue (Berger and Lo 2015), finding optimal solutions is computationally challenging, as proven to be NP-hard (Yu and LaValle 2013).

MRPP has been extensively studied in the context of multi-agent systems. Existing methods can be broadly classified into *coupled*, *decoupled*, and *dynamically-coupled* (Wagner and Choset 2015). The coupled approach (e.g., (Standley 2010), (Goldenberg et al. 2014)) does not scale with the number of robots, although they guarantee completeness and optimality. The decoupled approach (e.g., (Velagapudi, Sycara, and Scerri 2010), (Silver 2005)) reduces the search space for efficiency but does not provide theoretical guarantees. Dynamically-coupled methods (e.g., (Sharon et al. 2015), (Wagner and Choset 2015)) combine the advantages of the former two by coupling robots only whenever necessary. However, these methods often struggle to scale and require discretizing continuous environments,

Copyright © 2025, Association for the Advancement of Artificial Intelligence (www.aaai.org). All rights reserved.

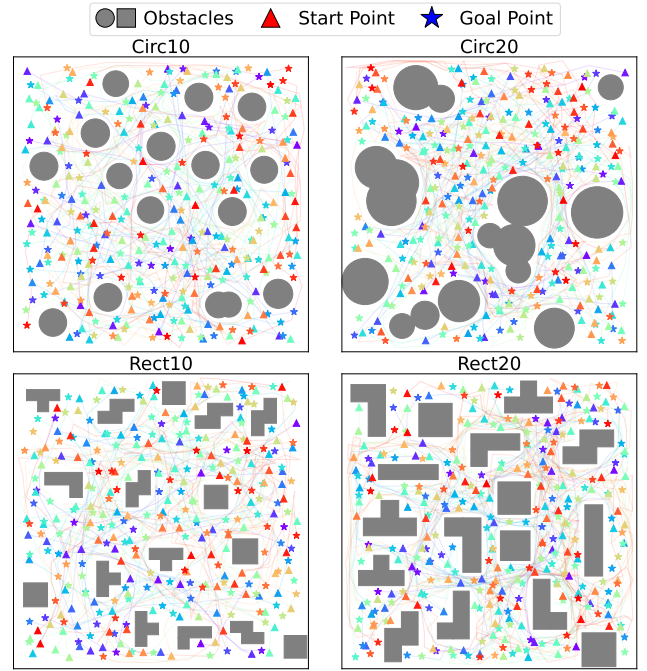


Figure 1: Challenging instances with 160 robots where robots often experience conflicts. These are also test environments Circ10, Circ20, Rect10, and Rect20 used in our experiments.

leading to suboptimal or infeasible solutions when applied to real-world robotic systems.

Our goal is to develop an efficient method for MRPP that can handle more than 100 robots in continuous space. We propose a two-level approach consisting of a low-level single-robot planner and a high-level conflict-resolving method. For the low level, we propose *Safe Interval RRT** (SI-RRT*), which borrows the concept of safe time intervals from Safe Interval Path Planning (SIPP) (Phillips and Likhachev 2011). While SIPP requires discretization of the environment, SI-RRT* allows a robot to navigate in continuous space without discrete time steps. The high level can use any conflict resolution method, such as Prioritized Planning (PP) and Conflict Based Search (CBS). We develop *Safe Interval Continuous-space PP* (SI-CPP) and *Safe Interval Continuous-space CBS* (SI-CCBS), which have their own advantages in computational efficiency and solution quality,

respectively.

The main contributions of the proposed method are (i) the improved scalability as SI-CPP can handle more than 160 robots in continuous space even in densely cluttered environments and (ii) theoretical guarantees for the probabilistic completeness and asymptotic optimality of SI-RRT*. (iii) In addition, we extend the proposed methods to consider the kinodynamic constraints of robots for real-world applications. We also provide extensive evaluations comparing our methods with state-of-the-art approaches such as SSSP (Okumura and Défago 2023), ST-RRT*-PP (Grothe et al. 2022), and Graph Transformer (Yu et al. 2023) in terms of computational efficiency and solution quality.

Related Work

SIPP (Phillips and Likhachev 2011) is an efficient single-robot path planner that can avoid dynamic obstacles. A *safe interval* is defined as a time period for a specific configuration during which no collision occurs. Since the number of safe intervals is significantly smaller than the number of time steps, SIPP effectively reduces the dimensionality of the problem. Nevertheless, as SIPP is designed for discrete space, it has limitations in handling robots that operate in continuous spatial and temporal spaces.

ST-RRT* (Grothe et al. 2022) is a bidirectional planner working in a space-time configuration space, which consists of Cartesian coordinates and a time dimension. PP (Orthey, Akbar, and Toussaint 2020) is used to resolve conflicts, where robots with lower priority modify their individual paths to avoid higher-priority robots. Since the search space has a time dimension, the robots can exploit temporality for more effective collision avoidance. Although PP does not guarantee deadlock-free paths, ST-RRT*-PP exhibits remarkable scalability and high-quality solutions.

Simultaneous Sampling and Search Planning (SSSP) (Okumura and Défago 2023) is a unified approach that does not separate the roadmap construction and conflict resolution. SSSP not only finds solutions quickly but also guarantees probabilistic completeness. However, the solution of SSSP is *sequential*, meaning that only one robot can move each time. A postprocessing method is necessary to make multiple robots move simultaneously, which requires additional computations. The probabilistic completeness would not hold for this post-processed solution.

In (Yu et al. 2023), a Graph Transformer (GT) is used as a heuristic function to accelerate CBS in non-grid settings, aiming for completeness and bounded-suboptimality. A contrastive loss training objective is introduced for learning a heuristic that ranks search nodes, demonstrating the generalizability of the method with promising results in accelerating CBS. While the approach of learning the heuristic function is novel, the success rate of the search decreases significantly as the number of robots increases.

Among the existing methods, ST-RRT*-PP is the most scalable and practical for MRPP or multi-agent pathfinding (MAPF) in continuous space. We aim to develop a more efficient algorithm with improved solution quality and scalability, particularly for large numbers of robots in complex

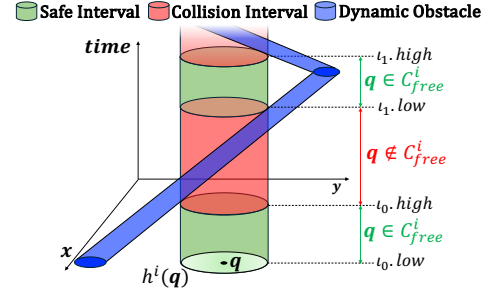


Figure 2: An illustration of the safe interval at q . The interval is defined for $h^i(q)$ to consider the size of robot i at q . The robot can stay at q without a collision during the safe interval (green). The shapes of the robot and dynamic obstacles, as well as the trajectory of the obstacle, can be arbitrary.

environments, to push the limit of the current state-of-the-art methods.

Problem Definition

We consider the MRPP problem of finding collision-free trajectories for k robots navigating from their start locations to respective goal locations in a *workspace* $\mathcal{W} \subset \mathbb{R}^d$ where $d \in \{2, 3\}$. A point $w \in \mathcal{W}$ can be occupied by an obstacle where the sets of static and dynamic obstacles are \mathcal{O}_S and \mathcal{O}_D , respectively. We assume that \mathcal{O}_S and \mathcal{O}_D are known. The *free workspace* is $\mathcal{W}^f = \mathcal{W} \setminus \mathcal{O}$ where $\mathcal{O} = \mathcal{O}_S \cup \mathcal{O}_D$. The *configuration space* (C-space) $\mathcal{C}^i \subseteq \mathcal{W}$ is the set of configurations of robot i . For a configuration $q \in \mathcal{C}^i$, the set of points occupied by i at q is denoted as $h^i(q) \subset \mathcal{W}$, where $h^i(q)$ depends on the shape of robot i . The free C-space (*free space*) is $\mathcal{C}_{\text{free}}^i = \{q \in \mathcal{C}^i \mid h^i(q) \cap \mathcal{O} = \emptyset\}$. A trajectory of robot i is a continuous function $\pi^i : [0, t_{\text{final}}^i] \rightarrow \mathcal{C}_{\text{free}}^i$ where t_{final}^i means the last time of the trajectory of i . Each configuration q in a trajectory is given by $\pi^i(t)$ for $t \in [0, t_{\text{final}}^i]$.

A *safe interval* (SI) of a configuration q is a continuous time period $\iota = [\text{low}, \text{high})$ during which the robot can remain at q without collisions, meaning q resides in $\mathcal{C}_{\text{free}}^i$ throughout ι . For convenience, we use $\iota.\text{low}$ and $\iota.\text{high}$ to denote the start and end times of this interval. Within this SI, the robot cannot arrive at q earlier than $\iota.\text{low}$ and must leave q no later than $\iota.\text{high}$ to avoid collisions. Conversely, a *collision interval* (CI) for q is a time period during which the robot at q would collide with at least one obstacle (i.e., a period when $q \notin \mathcal{C}_{\text{free}}^i$). An arbitrary time period for any q can be partitioned into alternating SIs and CIs depending on the trajectories of dynamic obstacles. In Fig. 2, the points occupied by robot i (i.e., $h^i(q)$) are depicted as a circle, which can represent any arbitrary shape. Green zones denote SIs where $h^i(q) \cap \mathcal{O} = \emptyset$ and red zones indicate CIs when the dynamic obstacle (blue) intersects $h^i(q)$.

Unlike the discrete space with finite states, a continuous space has an unbounded number of configurations. Since we cannot enumerate all SIs, we construct a *safe interval map* \mathcal{M} to store SIs whenever necessary. An SI at q is added to \mathcal{M} only if q is considered during the planning process.

For robot i , we define a roadmap (or a tree) $G^i = (\mathcal{V}, \mathcal{E})$ which is a connected topological graph within a $(d + 1)$ dimensional space where the last one dimension represents

time. A vertex $v \in \mathcal{V}$ in G^i corresponds to a specific configuration q and its earliest arrival time $v.t_{\text{low}}$, indicating that the robot cannot reach this configuration earlier than t_{low} . An edge $e \in \mathcal{E}$ connects a pair of vertices in \mathcal{V} if a feasible trajectory exists between their respective configurations, given the SIs of these configurations.

A *conflict* $\langle i, j, h^i(\pi^i(t)), h^j(\pi^j(t)) \rangle$ is defined for robots i and j for $t \in [t_s, t_e]$ where $h^i(\pi^i(t))$ represents the area occupied by i at t while i moves along π^i . Robots i and j collide within $[t_s, t_e]$ so $h^i(\pi^i(t)) \cap h^j(\pi^j(t)) \neq \emptyset$ for $t \in [t_s, t_e]$. A *constraint* for robot i is $\langle i, h^j(\pi^j(t)), t \rangle$ where $t \in [t_s, t_e]$ indicating that robot i must avoid $h^j(\pi^j(t))$ during $[t_s, t_e]$. In other words, robot i must generate a trajectory while satisfying $h^i(\pi^i(t)) \cap h^j(\pi^j(t)) = \emptyset$ for $t \in [t_s, t_e]$.

For a single robot i , we aim to find a collision-free trajectory π^i from the start configuration q_{start}^i to the goal configuration q_{goal}^i with the minimum arrival time t_{final}^i . For multiple robots, we aim to find collision-free trajectories for all k robots while minimizing the *flowtime* κ , which is the sum of individual arrival times of all robots at their goal configurations. We also aim to have a small *makespan* τ , which is the elapsed time until all robots reach their goals. They are defined as $\kappa = \sum_{i=1}^k t_{\text{final}}^i$ and $\tau = \max\{t_{\text{final}}^i | t_{\text{final}}^i \in \mathbb{R}, 1 \leq i \leq k\}$, respectively. The collision-free trajectories satisfy $h^i(\pi^i(t)) \cap h^j(\pi^j(t)) = \emptyset \forall i, j, i \neq j, \forall t \in [0, t_{\text{final}}]$ where $t_{\text{final}} = \max\{t_{\text{final}}^1, \dots, t_{\text{final}}^k\}$.

Single-Robot Planner: Safe Interval RRT*

We begin with proposing a sampling-based planner SI-RRT* for individual robots, which does not need to simplify the environment by discretizing the space and time. Also, fewer samples are needed to find high-quality trajectories compared to existing methods. For convenience, we temporarily omit the robot index (e.g., i) throughout this section.

SI-RRT* expands G up to *iteration* times to find a collision-free trajectory $\pi(t)$ for $t \in [t_{\text{start}}, t_{\text{goal}}]$. Once a solution is found, it continues improving it with more samples within the *iteration* limit. Here, t_{start} and t_{goal} represent the times at q_{start} and q_{goal} of the robot, respectively. These configurations belong to vertices v_{start} and v_{goal} of G .

Functions for tree expansion

Functions SAMPLING and STEER are used to grow G . SAMPLING randomly selects q_{rand} from \mathcal{C} with a probability of $1 - \lambda$ or the goal configuration q_{goal} with a probability of λ where $\lambda \in [0, 1]$. STEER attempts to generate a new configuration q_{new} . It identifies v_{near} in G whose configuration $v_{\text{near}}.q$ is the nearest to q_{rand} . If the distance between these two configurations is within a threshold d_{max} , q_{new} is set to q_{rand} . Otherwise, q_{new} is placed along the line segment connecting $v_{\text{near}}.q$ and q_{rand} , at a distance of d_{max} from $v_{\text{near}}.q$. STEER performs collision checking. If the trajectory from $v_{\text{near}}.q$ to q_{new} results in a collision with any obstacle in \mathcal{O} , it returns NULL. Otherwise, it returns q_{new} .

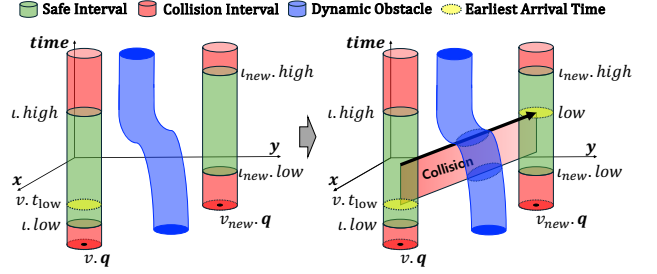


Figure 3: An illustration showing how *low* is determined in CHOOSEPARENT. (Left) The robot can stay v from $v.t_{\text{low}}$ until $v.t_{\text{high}}$ without collisions. The SI of $v_{\text{new}}.q$ is $[t_{\text{new}}.low, t_{\text{new}}.high]$. (Right) The bold arrow represents a trajectory to move from $v.q$ to $v_{\text{new}}.q$ as early as possible without colliding with the blue dynamic obstacle. Thus, *low* is the earliest arrival time at $v_{\text{new}}.q$ along the trajectory.

Functions for tree optimization

Functions GETNEIGHBOR, CHOOSEPARENT, and REWIRE are used to optimize G .¹ GETNEIGHBOR returns the set of nearby vertices $\mathcal{V}_{\text{neighbor}}$ which are within d_{max} from q_{new} . It performs collision checking to ensure that there is no collision between any pair of q_{new} and a vertex in $\mathcal{V}_{\text{neighbor}}$. CHOOSEPARENT returns a set of vertices \mathcal{V}_{new} for q_{new} where each $v_{\text{new}} \in \mathcal{V}_{\text{new}}$ is determined for each SI of q_{new} . For each v_{new} , it selects a parent from $\mathcal{V}_{\text{neighbor}}$ that minimizes $v_{\text{new}}.t_{\text{low}}$. REWIRE optimizes the tree structure of the roadmap G by potentially reassigning the parent vertices of the neighbors in $\mathcal{V}_{\text{neighbor}}$. For each neighbor, REWIRE checks if reassigning any $v_{\text{new}} \in \mathcal{V}_{\text{new}}$ as its new parent would result in an earlier arrival time. If so, the parent is updated accordingly.

In CHOOSEPARENT, a new set of vertices \mathcal{V}_{new} is initialized as empty. It iterates over all SIs associated with q_{new} , attempting to create a new vertex for each interval. For each SI t_{new} , v_{new} is created corresponding to q_{new} , with $t_{\text{low}} = \infty$ and no parent assigned. It then iterates over all vertices in $\mathcal{V}_{\text{neighbor}}$ to determine if any of them can serve as the parent vertex for v_{new} . For each $v \in \mathcal{V}_{\text{neighbor}}$, it checks for a collision-free trajectory from v to v_{new} within t_{new} . If found, the earliest possible arrival time at v_{new} is calculated and stored as *low*.

In the left of Fig. 3, the robot can stay at $v.q$ from $v.t_{\text{low}}$ until $v.t_{\text{high}}$ without collisions. The SI of $v_{\text{new}}.q$ (green) is $[t_{\text{new}}.low, t_{\text{new}}.high]$. In the right of Fig. 3, the bold arrow represents a trajectory to move from $v.q$ to $v_{\text{new}}.q$ as early as possible within their respective SIs while avoiding collisions with the dynamic obstacle (blue). Thus, the earliest arrival time at $v_{\text{new}}.q$ along this trajectory is assigned to *low*.

If t_{new} does not overlap with the time range during which the robot can reach $v_{\text{new}}.q$ from v , no feasible trajectory exists between them. Even with an overlap, a feasible trajectory may not exist if the trajectory from v to $v_{\text{new}}.q$ inevitably collides with a dynamic obstacle, regardless of when the robot departs. In either case, *low* cannot be de-

¹Owing to the space limit, we provide pseudocodes of these important subroutines CHOOSEPARENT and REWIRE as supplementary materials.

terminated, so the algorithm proceeds to the next vertex in $\mathcal{V}_{\text{neighbor}}$. If a valid low is found and lower than $v_{\text{new}}.t_{\text{low}}$, both the earliest arrival time and parent vertex of v_{new} are updated. Iterating over $\mathcal{V}_{\text{neighbor}}$ ensures v_{new} to get the earliest possible arrival time in the current tree structure. After checking all neighbors for each v_{new} , if a parent has been assigned to v_{new} (i.e., $v_{\text{new}}.t_{\text{low}} < \infty$), it is added to both \mathcal{V}_{new} and G . After processing all SIs of \mathbf{q}_{new} , \mathcal{V}_{new} is returned.

REWIRE optimizes G by reconnecting edges when better trajectories are possible, using \mathcal{V}_{new} from CHOOSEPARENT. For each $v_{\text{new}} \in \mathcal{V}_{\text{new}}$, it evaluates whether making v_{new} the parent of any $v \in \mathcal{V}_{\text{neighbor}}$ would decrease the earliest arrival time of v . This is done by computing the potential earliest arrival time at v when reaching it via v_{new} . If a valid low is found and earlier than $v.t_{\text{low}}$, then it updates $v.t_{\text{low}}$ to low and reassigns the parent of v to be v_{new} . This process iterates through all new vertices and their neighbors.

SI-RRT*

Based on the subroutines described above, SI-RRT* performs as described in Alg. 1. An SI map \mathcal{M} is initialized to be empty and then updated to add the SIs at $\mathbf{q}_{\text{start}}$ and \mathbf{q}_{goal} (lines 1–3). GETSAFEINTERVALS searches \mathcal{C} over time to find all SIs during which the given configuration is collision-free. The robot must reach \mathbf{q}_{goal} after all dynamic obstacles have cleared the area so as to the robot can remain at the goal indefinitely. Thus, the lower bound of the earliest arrival time at the goal node must exceed t_{lb} , the start of the last SI at \mathbf{q}_{goal} (line 4). Initialization of the vertices of the start and goal configurations follows (lines 5–6) where $v_{\text{goal}}.t_{\text{low}} = \infty$ as the arrival time at the goal has not been computed.

The main loop iterates for $iteration$ times (lines 7–28). If \mathbf{q}_{new} is found from SAMPLING and STEER, the SIs at \mathbf{q}_{new} are added to \mathcal{M} (line 13). If new vertices \mathcal{V}_{new} for \mathbf{q}_{new} are found by CHOOSEPARENT, REWIRE optimizes G (line 15–19). If (i) the configuration of v_{new} is equal to the goal configuration (line 21) and (ii) the robot could arrive at the goal at a time t such that $t_{\text{lb}} < t < v_{\text{goal}}.t_{\text{low}}$ (line 22), v_{goal} is updated by v_{new} . Once a goal vertex is found, Alg. 1 keeps optimizing G using CHOOSEPARENT and REWIRE until $iteration$ reaches zero. This feature enables SI-RRT* to balance the computational resources and solution quality. After all iterations, if v_{goal} has a parent, v_{goal} is connected to G so $\pi(t)$ is returned with the goal arriving time $t_{\text{final}} = v_{\text{goal}}.t_{\text{low}}$ (line 29–32). Otherwise, v_{goal} is not connected to G ; thus, NULL is returned (line 33).

Analysis of SI-RRT*

We prove the probabilistic completeness and the asymptotic optimality of SI-RRT*.

Theorem 1. *SI-RRT* is probabilistically complete.*

Proof. Let us consider \mathbf{q}_{new} and its $\mathcal{V}_{\text{neighbor}}$ in the roadmap G . For each v_{new} of \mathbf{q}_{new} , SI-RRT* attempts to create v_{new} and connect it to each $v \in \mathcal{V}_{\text{neighbor}}$. A connection between v_{new} and v is established unless either of the following conditions is met:

- (Condition 1) Non-overlapping safe intervals: If the interval resulting from linearly translating the SI of v by the moving time from $v.\mathbf{q}$ to \mathbf{q}_{new} does not overlap with

Algorithm 1: SI-RRT*

Input: $\mathcal{C}, \mathcal{C}_{\text{free}}, \mathcal{O}, G, \mathbf{q}_{\text{start}}, \mathbf{q}_{\text{goal}}, d_{\text{max}}, \lambda, iteration$

Output: Trajectory $\pi(t)$ or NULL

```

1:  $\mathcal{M} \leftarrow$  an empty map
2:  $\mathcal{M}[\mathbf{q}_{\text{start}}] \leftarrow \text{GETSAFEINTERVALS}(\mathbf{q}_{\text{start}}, \mathcal{C}_{\text{free}})$ 
3:  $\mathcal{M}[\mathbf{q}_{\text{goal}}] \leftarrow \text{GETSAFEINTERVALS}(\mathbf{q}_{\text{goal}}, \mathcal{C}_{\text{free}})$ 
4:  $t_{\text{lb}} \leftarrow \max\{low : (low, high) \in \mathcal{M}[\mathbf{q}_{\text{goal}}]\}$ 
5:  $v_{\text{start}}.\mathbf{q} \leftarrow \mathbf{q}_{\text{start}}, v_{\text{start}}.t_{\text{low}} \leftarrow 0, v_{\text{start}}.parent \leftarrow \text{NULL}$ 
6:  $v_{\text{goal}}.\mathbf{q} \leftarrow \mathbf{q}_{\text{goal}}, v_{\text{goal}}.t_{\text{low}} \leftarrow \infty, v_{\text{goal}}.parent \leftarrow \text{NULL}$ 
7: while  $iteration > 0$  do
8:    $\mathbf{q}_{\text{rand}} \leftarrow \text{SAMPLING}(\lambda, \mathbf{q}_{\text{goal}}, \mathcal{C})$ 
9:    $\mathbf{q}_{\text{new}} \leftarrow \text{STEER}(\mathbf{q}_{\text{rand}}, \mathcal{V})$ 
10:  if  $\mathbf{q}_{\text{new}} = \text{NULL}$  then
11:    continue
12:  end if
13:   $\mathcal{M}[\mathbf{q}_{\text{new}}] \leftarrow \text{GETSAFEINTERVALS}(\mathbf{q}_{\text{new}}, \mathcal{C}_{\text{free}})$ 
14:   $\mathcal{V}_{\text{neighbor}} \leftarrow \text{GETNEIGHBOR}(d_{\text{max}}, \mathcal{V})$ 
15:   $\mathcal{V}_{\text{new}} \leftarrow \text{CHOOSEPARENT}(\mathbf{q}_{\text{new}}, \mathcal{V}_{\text{neighbor}}, G, \mathcal{M}, \mathcal{O})$ 
16:  if  $\mathcal{V}_{\text{new}} = \emptyset$  then
17:    continue
18:  end if
19:   $\text{REWIRE}(\mathcal{V}_{\text{new}}, \mathcal{V}_{\text{neighbor}}, G, \mathcal{M}, \mathcal{O})$ 
20:  for  $v_{\text{new}}$  in  $\mathcal{V}_{\text{new}}$  do
21:    if  $v_{\text{new}}.\mathbf{q} = v_{\text{goal}}.\mathbf{q}$  then
22:      if  $t_{\text{lb}} < v_{\text{new}}.t_{\text{low}} < v_{\text{goal}}.t_{\text{low}}$  then
23:         $v_{\text{goal}} \leftarrow v_{\text{new}}$ 
24:      end if
25:    end if
26:  end for
27:   $iteration \leftarrow iteration - 1$ 
28: end while
29: if  $v_{\text{goal}}.parent \neq \text{NULL}$  then
30:    $t_{\text{final}} = v_{\text{goal}}.t_{\text{low}}$ 
31:   return  $\pi(t)$  for  $t \in [0, t_{\text{final}}]$ 
32: end if
33: return NULL

```

ι_{new} , the robot will inevitably collide with an obstacle, regardless of its departure time from v .

- (Condition 2) Unavoidable collisions: Even with overlapping safe intervals, if all trajectories from v to \mathbf{q}_{new} within ι_{new} collide with dynamic obstacles regardless of departure time, no feasible trajectory exists.

Based on these conditions, v_{new} is added to the tree if there exists at least one collision-free trajectory from any neighbor v to v_{new} within ι_{new} , satisfying both the time overlap and dynamic obstacle avoidance conditions. For each sampled configuration \mathbf{q}_{new} , SI-RRT* attempts to create \mathcal{V}_{new} for all of its SIs, ensuring comprehensive exploration of all feasible time windows. As sampling continues indefinitely, the tree progressively covers all reachable configurations and their associated SIs. This expansion results in a representation of all combinations of collision-free spatial and temporal configurations. The continuous expansion of G eventually ensures that SI-RRT* will connect v_{start} to v_{goal} if a feasible path exists. \square

Theorem 2. *SI-RRT* is asymptotically optimal.*

Proof. First, SI-RRT* maintains the earliest arrival time at each vertex in G . Therefore, the earliest arrival time at v_{goal} ,

which is $v_{\text{goal}} \cdot t_{\text{low}}$ (i.e., t_{final}), represents the minimum time to reach the goal within the structure of the current G . We can prove the asymptotic optimality of SI-RRT* based on the following two observations:

1. Representation optimality²: Once a solution is found, the trajectory $\pi(t)$ for $t \in [0, t_{\text{final}}]$ is optimal within the current representation of G .
2. Convergence to configuration space: As the number of samples increases, the set of vertices \mathcal{V} in roadmap G increasingly approximates $\mathcal{C}_{\text{free}}$.

Under infinite uniform sampling, G asymptotically covers all configurations in $\mathcal{C}_{\text{free}}$. Consequently, the representation converges to the solution space. Given that SI-RRT* is representation-optimal, the solution found from G approaches optimal as the number of samples approaches infinity. \square

An extension for kinodynamic constraints of robots

In real-world scenarios, physical robots are subject to various kinodynamic constraints. Our method can address these constraints by incorporating a local planner that finds trajectories under kinodynamic constraints between two states. Any local planner is acceptable if the planner can generate a collision-free trajectory connecting two states and guarantee the earliest possible arrival time at each destination state for a robot.

As an example, we implement *bang-bang transform* (LaValle, Sakcak, and LaValle 2023) for the local planner. With the planner, the robot accelerates at the maximum rate for a certain duration, navigates with its maximum velocity, and then decelerates until it reaches the next state with zero velocity. For each pair of states, we set the control input as $a_{\text{max}} = -a_{\text{min}} = 1$, calculate the velocity vector $\mathbf{v} = \mathbf{q}' - \mathbf{q}$, normalize it as $\hat{\mathbf{v}} = \mathbf{v}/|\mathbf{v}|$, and compute $s = \max_k(|\hat{v}_k|)$, $a_k = \hat{v}_k/s$, and $t = \sqrt{s|\mathbf{v}|}$, where k represents each dimension of the task space. It is worth noting that this implementation is merely an example of local planners that can handle kinodynamic constraints as various methods are available.

Furthermore, our method can deal with robots of different sizes and shapes. To show the capability, we randomly set different sizes for the robots in our implementation.³ The details of the implementation for kinodynamics and nonregular sizes can be seen in the video clip and the source code provided as supplementary materials.

Conflict resolution for multiple robots

As the high level manages conflicts between individual collision-free trajectories generated by the low-level SI-RRT*, we integrate PP and CBS with SI-RRT*, called SI-CPP and SI-CCBS, respectively. While SI-CPP is more efficient, SI-CCBS produces solutions with better quality, so

²The notion of being *representation-optimal*, also outlined in (Solis et al. 2021), entails achieving an optimal solution within a given representation of the solution space. The solution space is not necessarily identical to the representation.

³Robots with noncircular shapes can be represented by the circles circumscribing them.

one can choose either of them according to the requirements of the task.

Safe Interval Continuous-space PP (SI-CPP)

PP is a general approach based on a given, fixed priority of robots. Each robot avoids collisions with the trajectories of the higher-priority robots. Lower-priority robots treat the trajectories of higher-priority robots as dynamic obstacles when they plan the trajectories. Although PP is simple to implement and efficient, it is not complete. SI-CPP also inherits this property.

Safe Interval Continuous-space CBS (SI-CCBS)

CBS is an optimal and complete two-level algorithm. The high-level of SI-CCBS, following the structure of CBS, performs a best-first search in the Constraint Tree (CT). We adopt the cost function of the greedy variant of CBS proposed in (Barer et al. 2014), which is the number of conflicts between trajectories for fast search. To handle continuous space, we modify the definitions of conflicts and constraints.

SI-CCBS begins by inserting a root node with an empty constraint set into the search frontier *OPEN*. Each CT node contains the cost, individual trajectories, and constraints. The search iterates by expanding the node with the minimum cost from *OPEN*. The expanded node is eliminated from *OPEN*. If the expanded node has no conflict, the search terminates with a conflict-free solution. If *OPEN* is empty, the search fails to find a solution.

When expanding a CT node, conflicts among all trajectories are found and used to determine the cost of the node. To create the constraint set for a child CT node, we add a new constraint to the constraint set of the parent node. This new constraint is derived from a conflict (we choose the conflict with the smallest t) between the trajectories $\pi^i(t)$ and $\pi^j(t)$ of robots i and j , respectively. Subsequently, SI-RRT* finds new trajectories that abide by the updated constraint set. A child node updates its cost and trajectory set accordingly and is inserted into *OPEN*.

Experiments

First, we evaluate the performance of SI-RRT* for single-robot instances. Then, a comprehensive comparison of multi-robot planners follows to compare SI-CPP and SI-CCBS with others that are capable of handling continuous space and time. We have four test environments with different obstacle profiles: Circ10, Circ20, Rect10, and Rect20 as shown in Fig. 1. The size of all environments is $40\text{ m} \times 40\text{ m}$ where the radius of all robots is 0.5 m . Circ10 and Circ20 are filled with circular obstacles with different densities of the obstacles (10% and 20% of the entire space, respectively). Likewise, Rect10 and Rect20 are with rectangular obstacles. For each environment, we generate a set of 50 unique instances while randomizing the start and goal locations as well as the size and location of the obstacles. The parameter settings are as follows: $\lambda = 0.1$, $d_{\text{max}} = 5\text{ m}$, $\text{iteration} = 1500$, and the maximum velocity of the robots is 0.5 m/s . The system has an AMD Ryzen 5800X 3.8GHz CPU and 32G RAM, and all algorithms except for GT are implemented in C++17. GT is implemented using Python 3.8 because of its dependency on PyTorch.

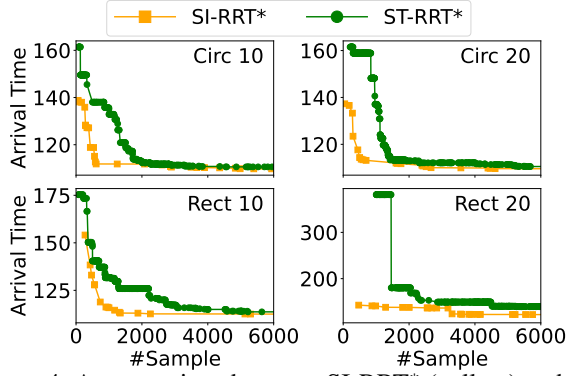


Figure 4: A comparison between SI-RRT* (yellow) and ST-RRT* (green) for single-robot path planning in the four test environments. The earliest arrival time at the goal of SI-RRT* decreases faster than ST-RRT*, indicating that SI-RRT* can find better trajectories faster.

Single-robot path planning

We compare SI-RRT* to ST-RRT*, one of the state-of-the-art sampling-based planners in continuous space with dynamic obstacles. ST-RRT* has been shown to outperform algorithms like RRT-Connect and RRT* in dynamic environments (Grothe et al. 2022). For comparison, we set up an environment with 60 dynamic obstacles with the same size and shape as the robot. The trajectories of the obstacles are randomly generated but known to both algorithms. We use the earliest arrival time at q_{goal} as our primary performance metric, reflecting search tree quality and trajectory efficiency. Specifically, a lower value indicates a better solution. To evaluate sample efficiency, we measure this metric while increasing the number of samples.

As shown in Fig. 4, SI-RRT* decreases the earliest arrival time at q_{goal} than ST-RRT* consistently across all environments. This suggests SI-RRT* discovers high-quality trajectories more quickly. The faster convergence of SI-RRT* stems from the dimensionality of the sampling space. SI-RRT* samples only in the spatial dimension while ST-RRT* samples from both spatial and temporal dimensions. Thus, SI-RRT* can cover more spatial configurations than ST-RRT* with the same number of samples. The performance gap increases in environments with more obstacles. If ST-RRT* rejects a sample owing to obstacles in the spatial dimension, resampling expands both the spatial and temporal dimensions of the search space, even though valid trajectories might exist without expanding the temporal dimension. The increased search space incurs inefficiency as more samples are needed to explore the spacial dimension. In contrast, SI-RRT* does not sample from the temporal dimension so can keep the search space smaller than ST-RRT*.

Multi-robot path planning

The metrics are the flowtime κ , makespan τ , and success rate. In congested environments, the importance of flowtime and makespan becomes evident as robots often need to wait to avoid conflicts with one another. The success rate is defined as the number of instances where a solution is found within five minutes out of all 50 test instances.

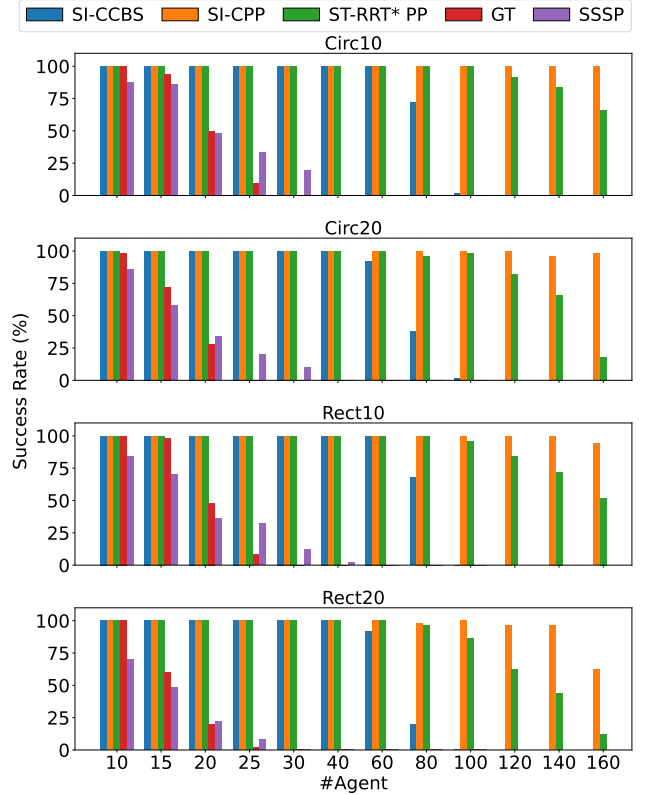


Figure 5: The success rates of compared methods under five minutes of the time limit. The proposed method SI-CPP succeeds in almost all instances, even in congested environments. As the advantage of SI-CCBS is in its solution quality, its success rates are lower than SI-CPP and ST-RRT*-PP but significantly higher than SSSP and GT.

We compare SI-CPP and SI-CCBS to ST-RRT* with ST-RRT*-PP, SSSP, and GT across the four test environments. We vary the number of robots up to 160. SSSP and GT operate in discrete time steps, requiring synchronization because robots must wait at waypoints until other robots arrive. In contrast, ST-RRT*-PP and our methods operate in continuous time, so synchronization is unnecessary.

The success rates shown in Fig. 5 demonstrate that SI-CPP, SI-CCBS, and ST-RRT*-PP are scalable. They maintain nearly 100% success rates for up to 60 robots. SI-CPP is notably scalable as it achieves 96% of the success rate even with 140 robots in the most challenging environment, Rect20. SI-CCBS maintains high success rates up to 60 robots but shows a decline for 80 robots in denser environments. ST-RRT*-PP is efficient, but its success rate declines with more than 100 robots. On the other hand, the scalability of SSSP and GT is limited. Their success rates drop significantly with more than 20 robots across all environments, especially in Circ20 and Rect20. Both methods fail to find solutions for problem instances beyond 40 robots.

Figs. 6 and 7 show comparisons of the solution quality of the compared algorithms for different robot team sizes. First, SSSP and GT exhibit significant performance drops as the problem size increases. The sequential movement of SSSP (discussed in the related work section) results in a rapid in-

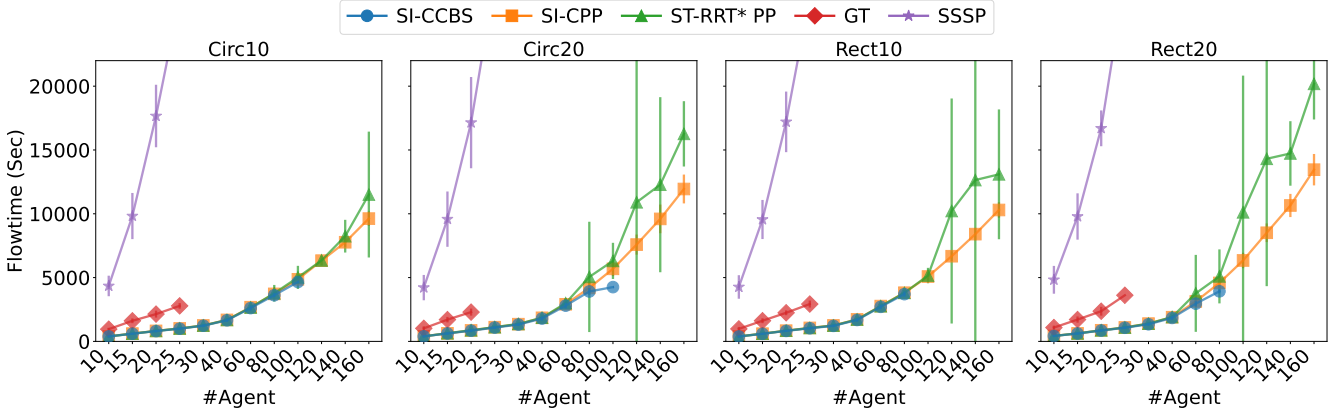


Figure 6: Compared flowtime where the standard deviation is displayed by the error bar in Circ10, Circ20, Rect10 and Rect20

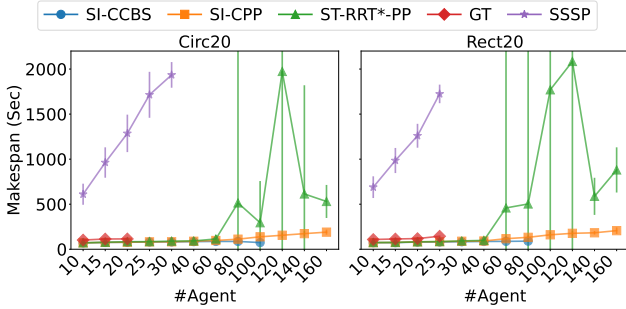


Figure 7: Compared makespans in Circ20 and Rect20

crease in flowtime. While GT shows a better performance than SSSP, its learning-based heuristic appears to be less effective in complex environments. Both methods yield substantially high flowtime and makespan values in most cases. From these results of SSSP and GT, we decide to focus on comparing our proposed methods (SI-CPP and SI-CCBS) with ST-RRT*-PP in the subsequent experiments.

For 60 robots, where all three methods maintain high success rates, SI-CCBS shows notable improvements. It achieves reductions of 6.48% and 21.4% in flowtime compared to ST-RRT*-PP in Circ20 and Rect20 environments, respectively. As we increase the number of robots to 100, the performance gap increases more significantly. SI-CPP reduces the flowtime 9.8% and 37.3% compared to ST-RRT*-PP in Circ20 and Rect20 environments, respectively.

Since we measure the flowtime and makespan for those only successful instances, they could be biased when the success rate is low, as only easy instances are likely to succeed. In instances with 160 robots, ST-RRT*-PP experiences a significant decline in the success rate. Nevertheless, SI-CPP outperforms ST-RRT*-PP in terms of the flowtime and makespan. Particularly, SI-CPP shows significant reductions in the flowtime in Circ20 and Rect20, which are 26.5% and 33.3%, respectively.

Furthermore, our methods show significant improvements in terms of makespan, particularly in large-size instances. With 60 robots, SI-CCBS reduces the makespan up to 23.9% in Circ20 and 80.9% in Rect20 compared to ST-RRT*-PP. For 120 robots, SI-CPP shows more significant reductions up to 92.12% in Circ20 and 91.51% in Rect20.

The standard deviations of the measured metrics provide additional insights. As the number of robots increases, ST-RRT*-PP exhibits a substantial growth in the standard deviation while SI-CPP and SI-CCBS maintain relatively low variability. These observations suggest that our methods are more consistent and reliable across diverse scenarios.

The superior performance of SI-RRT* in the solution quality can arise from its novel approach to edge connections. Unlike ST-RRT*, which samples in both spatial and temporal C-spaces, SI-RRT* samples only in the spatial C-space. In ST-RRT*, connecting vertex sampled in both space and time implicitly imposes velocity constraints due to fixed spatial and temporal distances between nodes. In contrast, the spatial-only sampling of SI-RRT* allows for determining unconstrained velocities between states, enabling the calculation of the earliest feasible arrival time at each destination. Consequently, SI-RRT* can generate more time-efficient trajectories, potentially minimizing overall travel time across the robot team.

In summary, SI-CCBS offers the highest quality solutions regarding flowtime and makespan, with reasonable scalability of up to 60 robots. SI-CPP balances the solution quality and scalability, maintaining high performance even for 160 robots in challenging environments. While ST-RRT*-PP shows comparable success rates in many instances, it is outperformed by our methods, particularly for larger team sizes and denser environments. Since we are unable to report all numbers from the experiments owing to the space limit, we attach them in the supplementary material.

Conclusion

We proposed a two-level approach for addressing the multi-robot path planning problem in continuous space to generate collision-free trajectories efficiently. Based on the sample-efficient SI-RRT*, two variants SI-CPP and SI-CCBS for MRPP were presented. Experiments demonstrated that SI-CPP outperforms a state-of-the-art method in terms of the success rate, which shows the scalability of SI-CPP given a time budget for computation. SI-CPP also shows a significantly smaller makespan. SI-CCBS outperforms the state-of-the-art method regarding the solution quality while not sacrificing the scalability significantly. As a future direction, we plan to run experiments with physical robots.

References

- Barer, M.; Sharon, G.; Stern, R.; and Felner, A. 2014. Sub-optimal variants of the conflict-based search algorithm for the multi-agent pathfinding problem. In *Proc. of International Symposium on Combinatorial Search*, volume 5, 19–27.
- Berger, J.; and Lo, N. 2015. An innovative multi-agent search-and-rescue path planning approach. *Computers & Operations Research*, 53: 24–31.
- Goldenberg, M.; Felner, A.; Stern, R.; Sharon, G.; Sturtevant, N.; Holte, R. C.; and Schaeffer, J. 2014. Enhanced partial expansion a. *Journal of Artificial Intelligence Research*, 50: 141–187.
- Grothe, F.; Hartmann, V. N.; Orthey, A.; and Toussaint, M. 2022. ST-RRT*: Asymptotically-Optimal Bidirectional Motion Planning through Space-Time. In *Proc. of International Conference on Robotics and Automation*, 3314–3320.
- LaValle, A. J.; Sakcak, B.; and LaValle, S. M. 2023. Bang-Bang Boosting of RRTs. In *Proc. of IEEE/RSJ International Conference on Intelligent Robots and Systems*, 2869–2876.
- Okumura, K.; and Défago, X. 2023. Quick Multi-Robot Motion Planning by Combining Sampling and Search. In *Proc. of International Joint Conferences on Artificial Intelligence*.
- Orthey, A.; Akbar, S.; and Toussaint, M. 2020. Multilevel motion planning: A fiber bundle formulation. *arXiv preprint arXiv:2007.09435*.
- Phillips, M.; and Likhachev, M. 2011. Sipp: Safe interval path planning for dynamic environments. In *Proc. of IEEE International Conference on Robotics and Automation*, 5628–5635.
- Sharon, G.; Stern, R.; Felner, A.; and Sturtevant, N. R. 2015. Conflict-based search for optimal multi-agent pathfinding. *Artificial Intelligence*, 219: 40–66.
- Silver, D. 2005. Cooperative pathfinding. In *Proc. of AAAI Conference on Artificial Intelligence and Interactive Digital Entertainment*, volume 1, 117–122.
- Solis, I.; Motes, J.; Sandström, R.; and Amato, N. M. 2021. Representation-optimal multi-robot motion planning using conflict-based search. *IEEE Robotics and Automation Letters*, 6: 4608–4615.
- Standley, T. 2010. Finding optimal solutions to cooperative pathfinding problems. In *Proc. of the AAAI Conference on Artificial Intelligence*, volume 24, 173–178.
- Stern, R.; Sturtevant, N.; Felner, A.; Koenig, S.; Ma, H.; Walker, T.; Li, J.; Atzmon, D.; Cohen, L.; Kumar, T.; et al. 2019. Multi-agent pathfinding: Definitions, variants, and benchmarks. In *Proc. of International Symposium on Combinatorial Search*, volume 10, 151–158.
- Varambally, S.; Li, J.; and Koenig, S. 2022. Which mapf model works best for automated warehousing? In *Proc. of International Symposium on Combinatorial Search*, volume 15, 190–198.
- Velagapudi, P.; Sycara, K.; and Scerri, P. 2010. Decentralized prioritized planning in large multirobot teams. In *Proc. of IEEE/RSJ International Conference on Intelligent Robots and Systems*, 4603–4609.
- Wagner, G.; and Choset, H. 2015. Subdimensional expansion for multirobot path planning. *Artificial intelligence*, 219: 1–24.
- Yu, C.; Li, Q.; Gao, S.; and Prorok, A. 2023. Accelerating Multi-Agent Planning Using Graph Transformers with Bounded Suboptimality. In *Proc. of International Conference on Robotics and Automation*.
- Yu, J.; and LaValle, S. 2013. Structure and intractability of optimal multi-robot path planning on graphs. In *Proc. of AAAI Conference on Artificial Intelligence*, volume 27, 1443–1449.

Supplementary Material

In this document, we provide (i) detailed explanations of the proposed algorithms that were omitted from the manuscript (ChooseParent and Rewire) due to space constraints, (ii) numerical results of the experiments, and (iii) additional experimental validations conducted in dynamic simulations. The accompanying video clip includes test instances performed in both the test environment described in the manuscript and the dynamic simulation environment.

I. DETAILED EXPLANATIONS OF CHOOSEPARENT AND REWIRE

In CHOOSEPARENT (Alg. 1), a new set of vertices, \mathcal{V}_{new} , is initialized as empty (line 1). Alg. 1 iterates over all safe intervals associated with \mathbf{q}_{new} , attempting to create a new vertex for each interval (line 2). For each safe interval ι_{new} , a new vertex v_{new} is initialized with its configuration set to \mathbf{q}_{new} , its earliest arrival time t_{low} set to infinity, and its parent vertex set to NULL (line 3). The algorithm then iterates through $\mathcal{V}_{\text{neighbor}}$ (line 4) to determine if any of them can serve as the parent vertex for v_{new} . For each neighboring vertex v , the algorithm checks if there exists a collision-free trajectory from v to v_{new} within the safe interval ι_{new} . If such a collision-free trajectory exists, the earliest possible arrival time at v_{new} is calculated and stored in the variable low (line 5).

Algorithm 1 CHOOSEPARENT

Input: \mathbf{q}_{new} , $\mathcal{V}_{\text{neighbor}}$, G , \mathcal{M} , \mathcal{O}

Output: \mathcal{V}_{new}

```

1:  $\mathcal{V}_{\text{new}} \leftarrow \emptyset$ 
2: for  $\iota_{\text{new}}$  in  $\mathcal{M}(\mathbf{q}_{\text{new}})$  do
3:    $v_{\text{new}}.\mathbf{q} \leftarrow \mathbf{q}_{\text{new}}$ ,  $v_{\text{new}}.t_{\text{low}} \leftarrow \infty$ ,  $v_{\text{new}}.\text{parent} = \text{NULL}$ 
4:   for  $v$  in  $\mathcal{V}_{\text{neighbor}}$  do
5:      $low \leftarrow$  the earliest arrival time of  $v_{\text{new}}.\mathbf{q}$  within  $[\iota_{\text{new}}.low, \iota_{\text{new}}.high)$  without colliding with  $\mathcal{O}$  when the robot moves from  $v$ , considering the execution time required to move from  $v$  to  $v_{\text{new}}$ 
6:     if  $low$  does not exist then
7:       continue
8:     end if
9:     if  $low < v_{\text{new}}.t_{\text{low}}$  then
10:       $v_{\text{new}}.t_{\text{low}} \leftarrow low$ 
11:       $v_{\text{new}}.\text{parent} \leftarrow v$ 
12:    end if
13:  end for
14:  if  $v_{\text{new}}.\text{parent} \neq \text{NULL}$  then
15:     $\mathcal{V}_{\text{new}} \leftarrow \mathcal{V}_{\text{new}} \cup v_{\text{new}}$ 
16:     $\mathcal{V} \leftarrow \mathcal{V} \cup v_{\text{new}}$ 
17:     $\mathcal{E} \leftarrow \mathcal{E} \cup (v_{\text{new}}, v_{\text{new}}.\text{parent})$ 
18:  end if
19: end for
20: return  $\mathcal{V}_{\text{new}}$ 

```

In the left of Fig. 3 of the manuscript, the robot can stay at configuration $v.\mathbf{q}$ from time $v.t_{\text{low}}$ until time $v.high$ without collisions. The safe interval of $v_{\text{new}}.\mathbf{q}$ (green) is $[\iota_{\text{new}}.low, \iota_{\text{new}}.high)$. In the right of Fig. 3 in the manuscript, the bold arrow represents a potential trajectory for the robot to move from $v.\mathbf{q}$ to $v_{\text{new}}.\mathbf{q}$ as early as possible while avoiding collisions with the dynamic obstacle (blue). Thus, the calculated earliest arrival time at configuration $(v_{\text{new}}.\mathbf{q})$ along this collision-free trajectory is assigned to the variable low .

If the safe interval ι_{new} of $v_{\text{new}}.\mathbf{q}$ does not overlap with the time range in which the robot can reach $v_{\text{new}}.\mathbf{q}$ from v , no feasible trajectory exists between them. Even with overlapping time ranges, a feasible trajectory may not exist if the trajectory from v to $v_{\text{new}}.\mathbf{q}$ inevitably collides with a dynamic obstacle, regardless of departure time. In both cases, a valid earliest arrival time low cannot be determined. When low is not found, the algorithm moves to the next neighboring vertex in $\mathcal{V}_{\text{neighbor}}$ (line 7). If a valid low is found and it is lower than the current earliest arrival time for v_{new} , both the arrival time and parent vertex of v_{new} are updated (lines 9–12). Iterating over $\mathcal{V}_{\text{neighbor}}$ ensures v_{new} is assigned the earliest possible arrival time within the current tree structure. If v_{new} has a parent, indicating a viable path, it is added to both \mathcal{V}_{new} and G (lines 14–18).

REWIRE (Alg. 2) optimizes G by reconnecting edges when better trajectories are possible, using the set \mathcal{V}_{new} from CHOOSEPARENT. For each $v_{\text{new}} \in \mathcal{V}_{\text{new}}$, it evaluates whether making v_{new} the parent of any $v \in \mathcal{V}_{\text{neighbor}}$ would lower earliest arrival time of v . This is done by computing the potential earliest arrival time at v when reaching it via v_{new} (line 4). If a valid earliest

Algorithm 2 REWIRE

Input: $\mathcal{V}_{\text{new}}, \mathcal{V}_{\text{neighbor}}, G, \mathcal{M}, \mathcal{O}$ **Output:** None

```
1: for  $v_{\text{new}}$  in  $\mathcal{V}_{\text{new}}$  do
2:   for  $v$  in  $\mathcal{V}_{\text{neighbor}}$  do
3:     for  $\iota_{\text{neighbor}}$  in  $\mathcal{M}(v.q)$  do
4:        $low \leftarrow$  the earliest arrival time of  $v.q$  within  $[\iota_{\text{neighbor}}.low, \iota_{\text{neighbor}}.high)$  without colliding with  $\mathcal{O}$  when the robot moves from
        $v_{\text{new}}$ , considering the execution time required to move from  $v$  to  $v_{\text{new}}$ 
5:       if  $low$  does not exist then
6:         continue
7:       end if
8:       if  $low < v.t_{\text{low}}$  then
9:          $v.t_{\text{low}} \leftarrow low$ 
10:         $\mathcal{E} \leftarrow \mathcal{E} \setminus (v, v.parent)$ 
11:         $v.parent \leftarrow v_{\text{new}}$ 
12:         $\mathcal{E} \leftarrow \mathcal{E} \cup (v, v_{\text{new}})$ 
13:      end if
14:    end for
15:  end for
16: end for
```

arrival time low is found and earlier than the current earliest arrival time $v.t_{\text{low}}$, then the algorithm updates $v.t_{\text{low}}$ to low and reassigns the parent of v to be v_{new} (lines 8–13). This process iterates through all new vertices and their neighbors.

II. NUMERICAL RESULTS OF THE EXPERIMENTS

In the manuscript, we were not able to include exact measured values due to the space constraint. In Table I, all numerical results are provided for all environments Circ10, Rect10, Circ20, and Rect20.

III. DYNAMIC SIMULATION

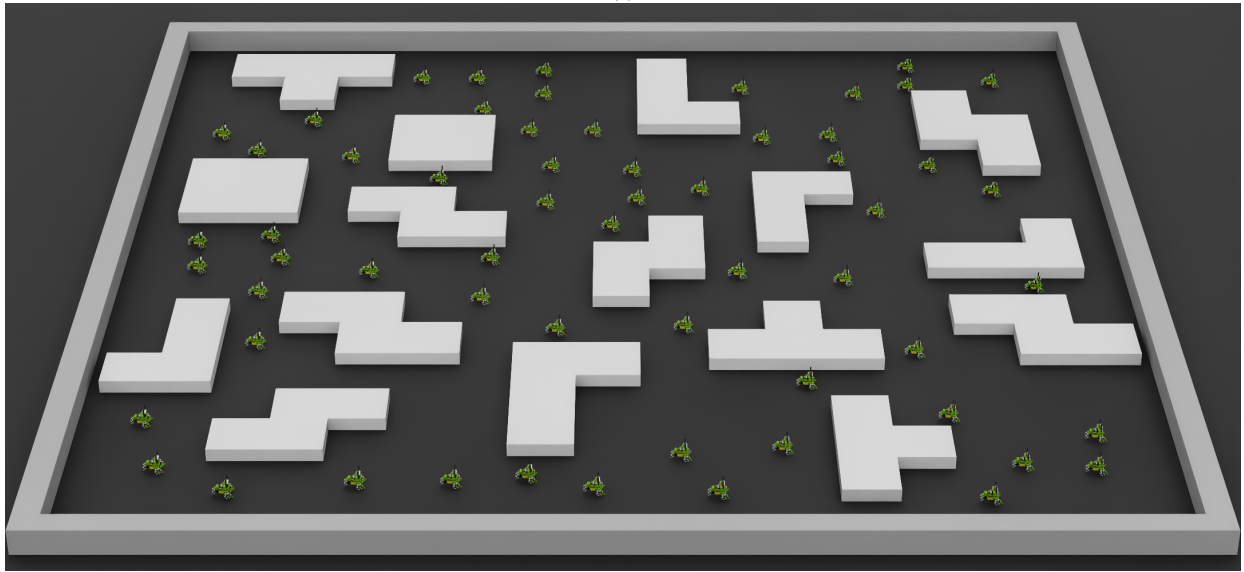
Since SI-RRT* assumes that robots move with a fixed velocity, the experimental results might be less convincing to use our methods for physical robots with complex dynamics. Thus, we executed our solutions from SI-CPP by robots in NVIDIA Isaac Sim (<https://developer.nvidia.com/isaac-sim>), a dynamic simulator with a high-fidelity physics engine. Since loading tens of robots in Isaac Sim is resource-intensive, we chose one of the simple robots, Kaya shown in Fig. 1a. We provide a safety margin of 20% of the radius of the robot for each robot, a reasonable setup in real-robot implementations. Given the computational resource of a PC with the exact specification in the main manuscript, we could reliably run 60 robots in Isaac Sim.

A solution of SI-CPP provides acceleration values to control velocity, along with the durations for acceleration and deceleration. The robots reach their destinations by accelerating and decelerating at the specified rates and times according to the given control inputs. Specifically, they accelerate at the determined rate for the specified duration and then decelerate at the determined rate for the specified duration. A solution is valid if no collision or deadlock occurs during the navigation. Among 20 test instances in the most challenging environment Rect20 (Fig. 1b), 100% of the solutions were turned out to be valid. The supplementary video includes two example executions in Circ20 and Rect20.

Overall, the execution result of solutions in dynamic simulation shows the feasibility of the proposed methods in real-world applications.



(a)



(b)

Fig. 1: (a) Kaya robot (omnidirectional) (b) A tested instance of **Rect20** with 60 robots in NVIDIA Isaac Sim

TABLE I: Measured metrics in the experiments of the manuscript

(a) Environments Circ10 and Rect10

Environment		Circ10					Rect10				
Metric	#robot	SI-CCBS	SI-CPP	ST-RRT*-PP	GT	SSSP	SI-CCBS	SI-CPP	ST-RRT*-PP	GT	SSSP
Success rate (%)	20	100	100	100	50	48	100	100	100	48	36
	40	100	100	100	0	0	100	100	100	0	2
	60	100	100	100	0	0	100	100	100	0	0
	80	72	100	100	0	0	68	100	100	0	0
	100	2	100	100	0	0	0	100	96	0	0
	120	0	100	92	0	0	0	100	84	0	0
	140	0	100	84	0	0	0	100	72	0	0
	160	0	100	66	0	0	0	94	52	0	0
Flowtime (sec)	20	806.16	823.20	819.38	2139.0	17662.1	821.35	839.85	835.92	2240.9	17202.5
	40	1653.05	1683.74	1679.72	-	-	1678.75	1720.40	1715.56	-	62920.9
	60	2610.41	2678.94	2655.26	-	-	2708.27	2766.59	2755.63	-	-
	80	3616.08	3723.15	3771.42	-	-	3701.48	3813.28	3801.57	-	-
	100	4655.82	4863.40	5015.05	-	-	-	5081.09	5158.74	-	-
	120	-	6327.18	6344.44	-	-	-	6674.42	10218.04	-	-
	140	-	7768.68	8244.31	-	-	-	8405.47	12642.75	-	-
	160	-	9622.02	11506.63	-	-	-	10297.65	13091.19	-	-
Sum of distance (m)	20	397.03	399.89	399.20	458.2	488.9	402.88	407.30	405.27	482.3	509.1
	40	793.14	802.56	801.70	-	-	800.53	812.18	810.99	-	953.2
	60	1218.09	1246.38	1239.95	-	-	1255.49	1281.13	1278.15	-	-
	80	1659.89	1707.72	1700.10	-	-	1681.96	1739.45	1728.62	-	-
	100	2111.40	2211.05	2213.59	-	-	-	2273.16	2257.23	-	-
	120	-	2807.80	2802.05	-	-	-	2898.26	2952.09	-	-
	140	-	3372.91	3418.93	-	-	-	3547.59	3628.51	-	-
	160	-	4070.74	4155.97	-	-	-	4230.00	4422.56	-	-
Makespan (sec)	20	73.34	73.82	73.56	106.9	1243.3	75.41	75.91	75.61	112.0	1283.3
	40	77.87	79.08	78.65	-	-	82.85	84.20	86.55	-	2387.0
	60	82.60	86.08	86.45	-	-	84.55	88.11	90.68	-	-
	80	84.67	88.92	111.96	-	-	85.23	95.89	102.26	-	-
	100	77.61	98.03	226.64	-	-	-	111.54	201.24	-	-
	120	-	110.11	125.12	-	-	-	137.06	1775.00	-	-
	140	-	133.60	345.70	-	-	-	151.38	1329.46	-	-
	160	-	153.98	1227.89	-	-	-	165.12	1344.00	-	-

(b) More difficult environments Circ20 and Rect20

Environment		Circ20					Rect20				
Metric	#robot	SI-CCBS	SI-CPP	ST-RRT*-PP	GT	SSSP	SI-CCBS	SI-CPP	ST-RRT*-PP	GT	SSSP
Success rate (%)	20	100	100	100	28	34	100	100	100	20	22
	40	100	100	100	0	0	100	100	100	0	0
	60	92	100	100	0	0	92	100	100	0	0
	80	38	100	96	0	0	20	98	96	0	0
	100	2	100	98	0	0	0	100	86	0	0
	120	0	100	82	0	0	0	96	62	0	0
	140	0	96	66	0	0	0	96	44	0	0
	160	0	98	18	0	0	0	62	12	0	0
Flowtime (sec)	20	837.47	857.39	873.1	2295.3	17142.9	850.38	870.72	866.1	2364.9	16696.4
	40	1791.15	1848.30	1854.0	-	-	1839.61	1893.12	1910.0	-	-
	60	2800.59	2907.90	2994.7	-	-	2955.70	3129.13	3763.5	-	-
	80	3911.63	4193.95	5052.9	-	-	3924.30	4581.84	5093.6	-	-
	100	4253.73	5685.72	6307.6	-	-	-	6341.40	10115.3	-	-
	120	-	7585.49	10901.93	-	-	-	8512.18	14308.43	-	-
	140	-	9599.20	12278.50	-	-	-	10650.45	14727.81	-	-
	160	-	11942.79	16263.49	-	-	-	13455.49	20182.43	-	-
Sum of distance (m)	20	410.34	416.08	417.6	443.5	507.9	410.11	418.53	413.6	468.6	507.3
	40	849.90	870.19	867.0	-	-	858.95	880.18	876.5	-	-
	60	1287.37	1335.40	1350.0	-	-	1325.91	1404.70	1400.8	-	-
	80	1758.10	1869.69	1899.5	-	-	1714.89	1968.39	1978.7	-	-
	100	1972.24	2448.97	2532.8	-	-	-	2629.45	2675.4	-	-
	120	-	3176.30	3328.48	-	-	-	3375.16	3688.02	-	-
	140	-	3871.72	4093.30	-	-	-	4090.95	4589.90	-	-
	160	-	4614.01	5201.03	-	-	-	4944.88	5598.63	-	-
Makespan (sec)	20	77.27	78.03	83.4	114.8	1286.1	79.88	82.14	82.4	118.2	1259.6
	40	84.49	88.75	92.6	-	-	86.36	91.58	98.1	-	-
	60	86.81	97.16	114.1	-	-	87.57	117.29	458.8	-	-
	80	86.64	111.95	514.2	-	-	89.80	132.38	502.7	-	-
	100	74.25	138.00	294.5	-	-	-	160.33	1769.9	-	-
	120	-	155.34	1973.52	-	-	-	176.82	2084.40	-	-
	140	-	173.34	613.73	-	-	-	182.75	587.23	-	-
	160	-	189.84	530.44	-	-	-	206.43	880.44	-	-